JOURNAL OF MATERIALS SCIENCE 10 (1975) 973–982

Investigation of phase intergrowth morphologies in the system Zn_2SiO_4–SiO_2 by photo-emission electron microscopy

L. WEBER, H. R. OSWALD
Anorganisch-Chemisches Institut der Universität, Zürich, Switzerland

By means of photo-emission electron microscopy, which is described briefly, X-ray diffraction and electron microprobe analysis the hypo- and hypereutectic solidification in the system Zn_2SiO_4–SiO_2 has been investigated. Faceted (idiomorphic) growth of stable α- and metastable β-zinc silicate with some excess SiO_2 on the hypoeutectic side of the phase diagram and a metastable region of liquid immiscibility on the SiO_2-rich (hypereutectic) side determine the respective phase intergrowth morphologies. Unconstrained eutectic solidification causes a "divorced eutectic" where the zinc silicate constituent grows first from the undercooled liquid, which is simultaneously enriched in SiO_2.

1. Introduction

Growth kinetics in eutectic systems with metals and semi-metals as constituents have already been studied extensively [1, 2]. In oxide systems, however, respective knowledge exists only to a limited extent [3]. In this paper the new method of photo-emission electron microscopy is described as a tool for metallography-like investigations of solid surfaces, and observations about intergrowth morphologies of phases in the eutectic system Zn_2SiO_4–SiO_2 are presented.

1.1. Photo-emission electron microscopy

Photo-emission electron microscopy (PEEM) is a useful method of getting a direct image of the chemical differences in a plane polished sample without any preceding etching.

Bombardment with photons emitted from high pressure mercury ultraviolet lamps expells electrons from the sample. These photo-electrons are accelerated in an electric field of 40 kV and enter a conventional electron-optical lens system. The resulting brightness contrast is recorded on a photographic plate and depends strongly on the chemical composition of the different phases. Although it is not possible at present to use the PEEM as a method for chemical analysis, it is very sensitive to inhomogeneities in materials. Owing to the small range below the surface where the photo-electrons come from ($\approx$ 100 Å), the actual resolving power in the case of non-metals amounts to about $\lesssim$ 0.1 μm. The available magnifications are restricted at present mainly by the intensity of the photo-electron current which is often very weak. The theoretical resolving power which may be verified by using special kinds of metals is about 200 Å. More detailed descriptions about PEEM and its application to metals have been given [4, 5], although reports of its application to ceramics and minerals are fewer [6, 7].

1.2. The ZnO–SiO_2 system

The phase diagram of the system ZnO–SiO_2 established by Bunting [8] is shown in Fig. 1. While Bunting only found one stable compound, α-Zn_2SiO_4, later works report the existence of two metastable polymorphs: β-Zn_2SiO_4 appears either after rapid cooling of liquid melts with compositions between 33.3 and 63 mol% SiO_2 or in the first steps of devitrification of glasses [9]. X-ray powder diagrams were registered and indexed earlier [10, 11]. Williamson and Glasser [9] studied metastable phase relations in this system: β-Zn_2SiO_4 is said to form mixed crystals containing up to 64% SiO_2.* This was concluded from X-ray powder diffraction evidence that β-

*Chemical composition is in mol% SiO_2 throughout.

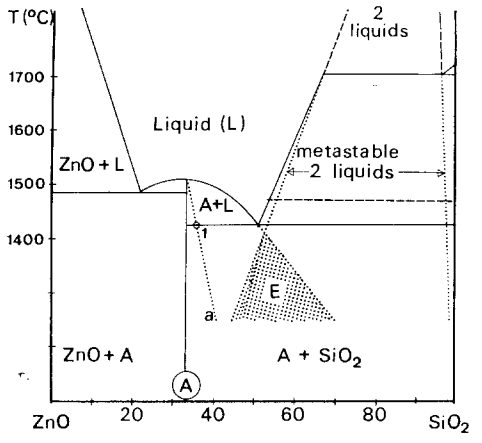

Figure 1 Stable phase diagram ZnO–SiO_2 with the compound Zn_2SiO_4 after Bunting [8], corrected by Williamson and Glasser [9]. Metastable phase relations as used in this work are drawn as dotted lines: line a is the approximate boundary of Zn_2SiO_4–SiO_2 solid solution (phase A) if grown from a rapidly cooled (condition 1) melt. Line a is supported by point 1 from microprobe measurements in large (> 10 μm) A-crystals (α-form). E = eutectic "coupled region".

Zn_2SiO_4 crystallized, but SiO_2 did not. Moreover, the optical refractive index of β-Zn_2SiO_4 varied continuously with composition as would be expected for a solid solution.

The existence of the γ-form seems to be less certain and its chemical composition (either Zn_2SiO_4 or $ZnSiO_3$) is unknown. After Williamson and Glasser [9] it was observed as globules within a glass matrix after very rapid quenching of liquid melts in the compositional range 45 to 55%. X-ray powder data have been indexed with a face centred cubic cell [9].

Zinc silicate may take up MnO (1 to 3%) which causes green and yellow luminescence of the α- and β-polymorphs, respectively. This property was the main reason for most of the earlier investigations [10, 12, 13].

2. Experimental procedure

Powder fractions of ZnO and SiO_2 as quartz (Merck LTD, Germany; impurity content <1 wt%) were intimately mixed in various molar portions, then pressed to tablets (0.8 g), put into small (8 mm diameter) covered platinum crucibles and melted in a tube oven held at the respective reaction temperature. After melting was complete, the samples were quickly removed from the oven and either immediately put on a cold metal plate (cooling condition 1) or allowed to cool in air (condition 2). By regulating the oven temperature, some samples were cooled much more slowly (2 to 5°C min^{-1} – condition 3 and 1 to 2°C min^{-1} – condition 4) across the eutectic temperature until arriving at about 1300 to 1350°C. The samples were then removed from the oven under condition 1. Moreover, quickly cooled melts (condition 1) were reheated at 1400 to 1420°C (condition 5) and at a lower temperature (1350°C, condition 6) for 60 to 80 min.

Cooling procedures 1 and 2 correspond approximately to the "medium quenching rate" used by Williamson and Glasser [9], thus allowing some comparison.

After cooling to room temperature, the samples had a plate-like form 7 to 8 mm diameter and about 1 to 2 mm thick. The lower side was then ground and polished to obtain a plane surface for PEEM investigation. The composition of the same surfaces was also measured by electron microprobe analysis as a loss of 2 to 3% ZnO occurred during melting. The crystalline phases present were determined by powder X-ray diffraction on a diffractometer and a Guinier camera (Cu$K\alpha$-radiation).

3. Results

The results are compiled in Table I. Typical examples of the resulting intergrowth morphologies revealed by PEEM are given in Figs. 2 to 16. The bright phase in these pictures is always α- or β-zinc silicate, since both polymorphs show strong absorption of ultraviolet light and, therefore, give a strong photoelectron emission, whereas SiO_2 is relatively transparent to ultraviolet light and is a poor emitter: SiO_2-rich phases, therefore, appear dark in the PEEM pictures.

4. Discussion

According to the theory of Jackson [14], the morphology of crystals grown from the melt may be correlated with a factor $\Delta S = \Delta H_f/R \cdot T_m$ where ΔH_f is the latent heat of fusion, R is the gas constant and T_m the melting temperature (K). ΔS is the molar entropy of fusion in dimensionless units.

Materials with $\Delta S < 1$ were found to grow isotropic or as metastable curved dendrites and cells. For $\Delta S > 4$ faceted growth is usual or faceted pseudo-dendrites, called "hoppers" after Hunt and Jackson [15]. In the present system Zn_2SiO_4–SiO_2 the values of ΔS amount to about

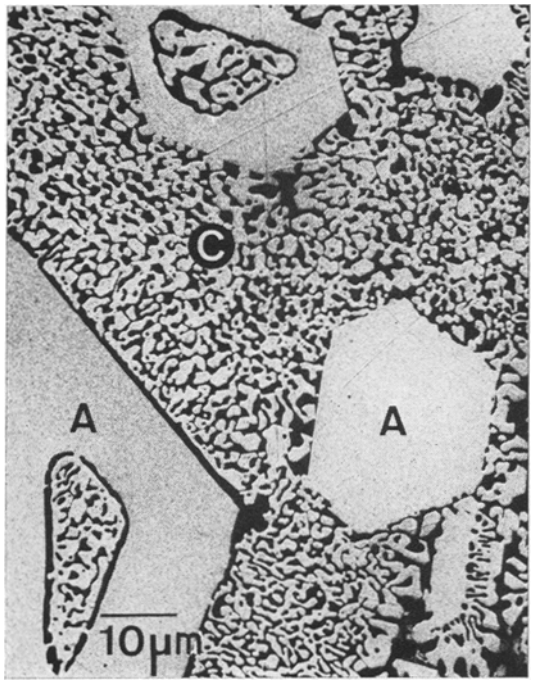

5.5 (Zn_2SiO_4) and 0.5 (SiO_2), with ΔH_f about 21 and 2 kcal, respectively. As a consequence, the former compound is expected to be the better nucleant and to grow in a faceted habit. SiO_2 is well known for its sluggishness of crystallization. During cooling SiO_2-rich melts behave as undercooled liquids with subsequent glass formation rather than showing crystallization [16].

4.1. Hypoeutectic solidification

Fig. 2 represents the PEEM image of a hypoeutectic composition (47%). Primary zinc silicate crystals have grown in the stable α-state at about 1440°C. Above the eutectic temperature they form mixed crystals to a limited extent (2 to 3% excess SiO_2 after microprobe measurements), whereas they segregate SiO_2 on a very fine scale if cooled to room temperature. Zinc silicate,

Figure 2 Primary crystallization of phase A (A, α-form) from hypoeutectic melt (47%) at 1440°C. Slow cooling (condition 3) causes a "divorced eutectic" structure (C) explained in Section 4.1.

TABLE I Experimental conditions and results

Bulk composition (mol % SiO_2)	Melting temperature (°C)	Melting time (min)	Cooling condition*	Morphological type by PEEM, see Fig.:	X-ray
37	1500	5	2	3, but much larger crystals	α-An_2SiO_4 + very little cristobalite
37	1530	3	2	3	As above
42	1440	45	2	4	As above
47	1440	30	2	4	As above
42	1550	6	1	5	α-Zn_2SiO_4
47	1440	10	3	2	α-Zn_2SiO_4 + little cristobalite
47	1550	6	1	6	β-Zn_2SiO_4
51	1530	4	1	10	Glassy, beginning β-Zn_2SiO_4
51	1500	5	3	13	β-Zn_2SiO_4
51	1460	4	4	11 + 12	α-Zn_2SiO_4 + some cristobalite
51	1500	3	5	14	α-Zn_2SiO_4 + cristobalite
51	1530	4	6	15	α-Zn_2SiO_4 + little cristobalite
52.5	1500	9	2	7	β-Zn_2SiO_4
52.5	1500	6	3	7, 8	β-Zn_2SiO_4 (+ cristobalite?)
54	1500	9	3	7, 8	β-Zn_2SiO_4 + little cristobalite
54	1500	7	2	7	β-Zn_2SiO_4
54	1500	6	6	16	α-Zn_2SiO_4 + cristobalite
59	1600	45	2	8	β-Zn_2SiO_4 (+ cristobalite?)
59	1620	45	1	10	Glassy, beginning β-Zn_2SiO_4
59	1620 + 1450	70 + 70	1	9	β-Zn_2SiO_4 + cristobalite
63	1600	85	2	9, but much larger cristobalite crystals	As above
68	1600	120	2	As above	As above
73	1600	165	2	As above	As above

*See Section 2 for definition.

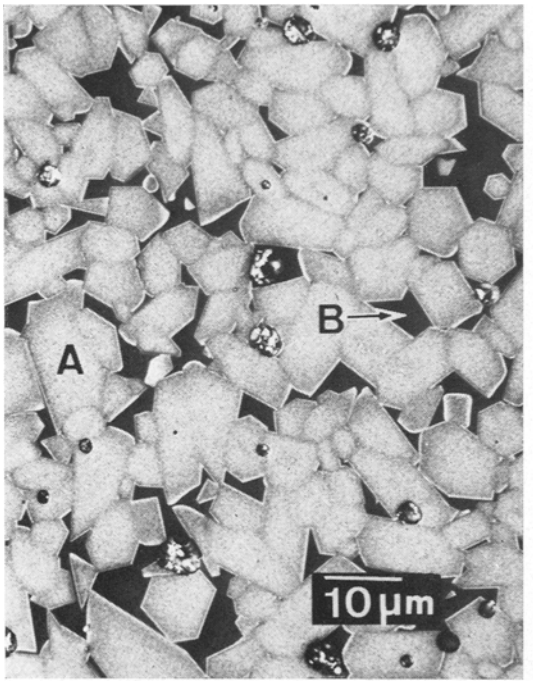

Figure 3 Phase A (A, α-form) grown from the melt (37%) during cooling (condition 2). Subsequent SiO_2-segregation (granular areas) points to the inhomogeneity of the former mixed crystals. Bright rims adjacent to the SiO_2-rich phase (B, dark) indicate the "degenerate eutectic" (see text).

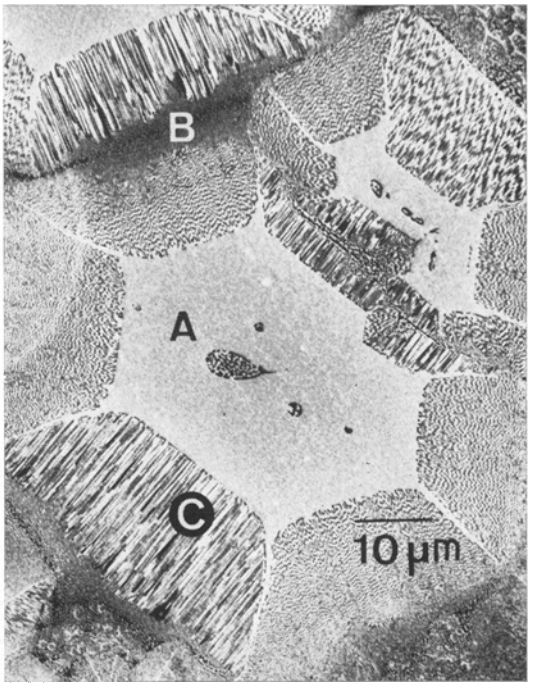

Figure 4 During cooling (condition 2) of a hypoeutectic sample (42%) after primary A-crystallization (A, α-form) at 1440°C, a fibre-like eutectic structure (C) develops with an area of great enrichment of SiO_2 in adjacent regions (B, dark).

either in the α or β form, with some excess SiO_2 is called phase A here. The SiO_2-rich phase according to the metastable boundary of immiscibility (Fig. 1) is called phase B.

A-crystals grown during quick cooling (condition 2) from the melt (37%) prove to be inhomogeneous with increasing SiO_2 from core to rim after SiO_2 segregation (Fig. 3). Below the eutectic temperature the little remaining eutectic-like liquid between the primary A-crystals separates by crystallization of purer zinc silicate onto primary A-crystals (bright rims, Fig. 3) leaving the SiO_2-rich constituent B in the interstitial regions ("degenerate eutectic").

It may be noticed that the interpretation of microstructures is limited by the fact that qualitative changes of the chemical composition, which are indicated sensitively by the brightness contrast in PEEM can often not be supported quantitatively by microprobe measurements, since the latter give no reliable analytical data for areas smaller than about 5 µm. If a hypoeutectic melt is cooled quickly (condition 2) after primary crystallization at 1440°C, the surfaces of primary A-crystals act as heterogeneous nucleation centres for rapid cellular (dendrite-like) growth of the eutectic A-constituent into the surrounding liquid. This effect was observed earlier in metals [18]. As A grows and the remaining liquid is enriched in SiO_2, this causes a considerable constitutional undercooling and gives rise to the fibre- or dendrite-like structure shown in Fig. 4. At the adjacent boundary regions, a large SiO_2 enrichment is often observed, similar to that at the end of a zone-refined sample. The same behaviour may be shown during slower cooling, but the primary A-crystals often become covered with a layer of SiO_2-rich phase (Fig. 2) so that they are less likely to cause heterogeneous nucleation.

A-crystals in the α-form (trigonal, $R\bar{3}$) tend to grow with distortion of their pseudo-hexagonal habit if the melt (42%) is cooled rapidly (condition 1) as shown in Fig. 5. The β-polymorph (triclinic indexed powder pattern after Williamson and Glasser [9], while we found a pseudo-hexagonal electron diffraction pattern) tends to even stronger distortion if grown from

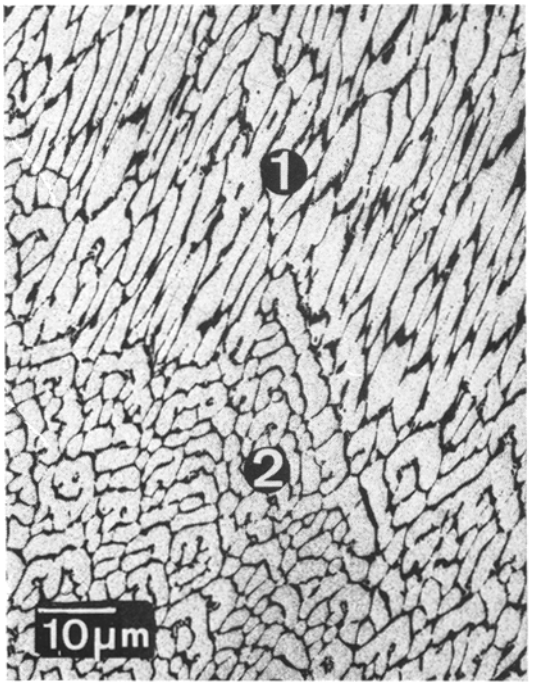

Figure 5 Phase A (α-form) grown during rapid cooling (condition 1) from the melt (42%) with distorted pseudo-hexagonal habit. The direction of distortion is approximately parallel (1) and perpendicular (2) to the image plane.

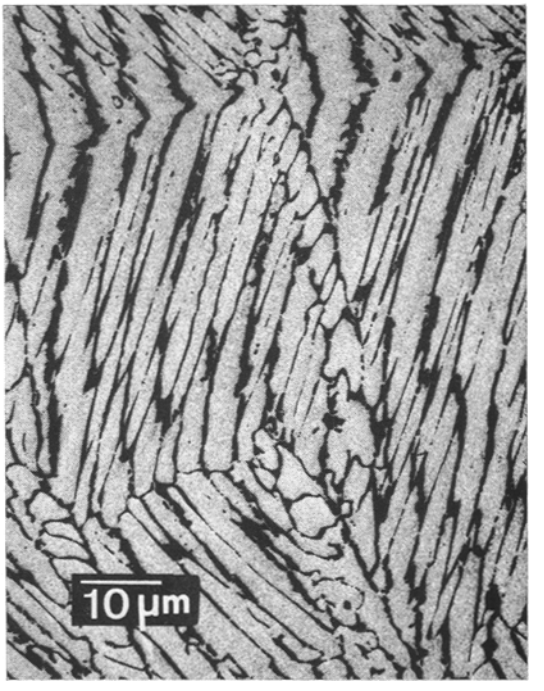

Figure 6 Phase A (β-form) grown during cooling (condition 1) from the melt (47%). The habit resembles that of the α-form and is strongly deformed to faceted pseudo-dendrites (hoppers).

the melt of 47% SiO_2 under the same cooling condition (Fig. 6). No real eutectic structure exists in both intergrowth morphologies and it may be concluded that the temperature at which crystallization stops is so low that the compositions of the rapidly grown A-polymorphs (according to line a, Fig. 1) are close to the respective compositions of the initial melts.

It was noticed that decreasing speed of undercooling was necessary to obtain the crystalline β-state of phase A, the more the chemical composition of a hypoeutectic melt approaches that of the eutectic. While the *d*-spacings of both A-polymorphs do not change in dependence on the kind of cooling history, the relative intensities within the X-ray pattern change very sensitively as has been observed by Williamson and Glasser [9].

X-ray evidence for the occurrence of crystalline SiO_2 after cooling conditions 1 to 3 can be detected only after careful examination. As a crystallization product of undercooled SiO_2-rich liquids, low-cristobalite appears [16]. The only reliable indication of its appearance is given by the (1 1 2)-peak at $2\theta = 36.4\text{-}5°$ (Cu radiation) if it occurs with α-Zn_2SiO_4, or (1 1 1) at $2\theta = 28.5°$ if it occurs with β-Zn_2SiO_4. Nearly all other peaks of low-cristobalite overlap with those of the Zn_2SiO_4 polymorphs.

The tendency to form cristobalite increases with decreasing cooling rate and with decreasing SiO_2 bulk content of the initial hypoeutectic melt (see below).

4.2. Hypereutectic solidification

If hypereutectic melts with compositions between 51 and 60% are cooled (condition 2) from about 1600°C, the typical structures which appear are shown in Figs. 7 and 8. The origin of these may be discussed using Fig. 1. The region of stable liquid immiscibility > 1700°C, extends metastably to lower temperatures giving a region of metastable liquid immiscibility below this temperature. Therefore, the undercooled melt separates into a large portion having nearly the eutectic composition and a smaller one of the amorphous phase B, the composition of which is assumed to be similar to the SiO_2-rich boundary of the miscibility gap. (No reliable quantitative microprobe analysis is possible because of the

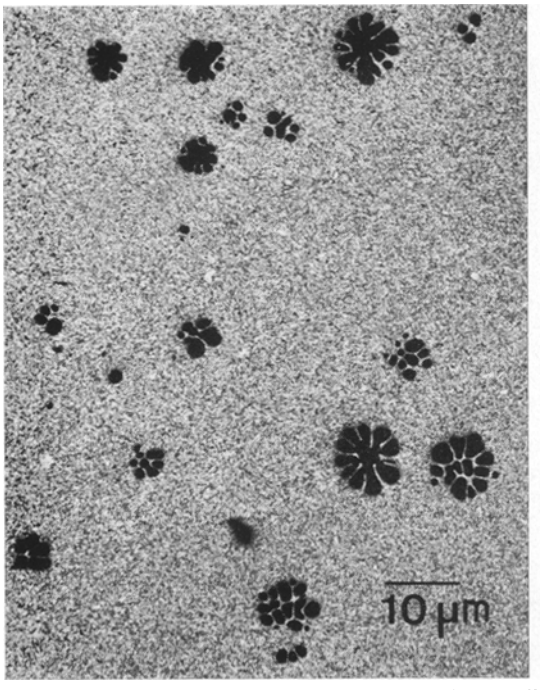

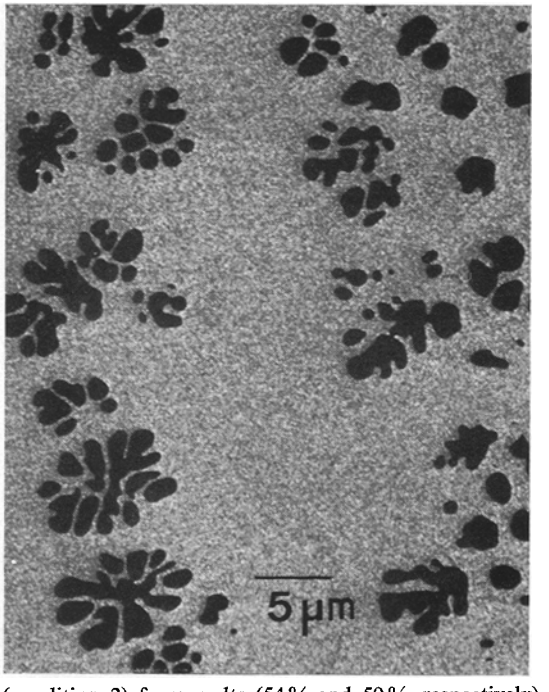

Figures 7 and 8 Hypereutectic morphology after cooling (condition 2) from melts (54% and 59%, respectively). Primary amorphous phase B (dark) forms a "flower pattern" and curved dendrites amid a very fine-scaled eutectic structure consisting of phase A (β-form) and amorphous B.

small size – $\lesssim$ 3 to 5 µm – of the B-particles, Figs. 7 and 8.)

The small globules of phase B may first join to form a flower pattern (Fig. 7) and by further growth, curved dendrites (Fig. 8). Only at lower cooling rates (condition 3) does faceted low-cristobalite crystallize. The larger part of the melt solidifies into a very finely divided eutectic structure consisting of phase A (β-form) and amorphous B. True primary faceted cristobalite grows (Fig. 9) if the temperature of the melt is held for about 1 h at 1450°C, i.e. above the eutectic temperature.

If hypereutectic melts are cooled very rapidly (condition 1) the resulting appearance is to that shown in Fig. 10, but the globules of phase B may be much smaller if the bulk composition is poorer in SiO_2. The sample shown in Fig. 10 proved to be mostly glass with only some weak and broad X-ray peaks indicating that β-zinc silicate was beginning to crystallize.

Under cooling conditions 1 to 3, only the metastable β-form of phase A was observed after solidification of hypereutectic melts (see Section 4.3).

It is obvious from PEEM observations that liquid phase separation begins immediately after a liquid composition penetrates the metastable liquid immiscibility region. Its boundary on the eutectic side is not far from the stable hypereutectic liquidus curve, as drawn in Fig. 1. The boundary appears to intersect the metastable extension of the hypoeutectic liquidus line at about 52.5%, as melts of this composition and those richer in SiO_2 behave as hypereutectics under the metastable cooling conditions used in this work.

It may be assumed that during hypoeutectic solidification phase separation also takes place in the residual liquid after primary crystallization at medium cooling rates (conditions 2 and 3). The smaller the amount of the liquid remaining (i.e. the smaller the SiO_2 content of the initial melt), the sooner it becomes enriched in SiO_2, thus coming into the compositional region of metastable liquid phase separation with subsequent crystallization of low-cristobalite. This was indicated by X-ray investigations as noted in Section 4.1.

4.3. Eutectic solidification

From a eutectic melt (51% SiO_2) cooled very

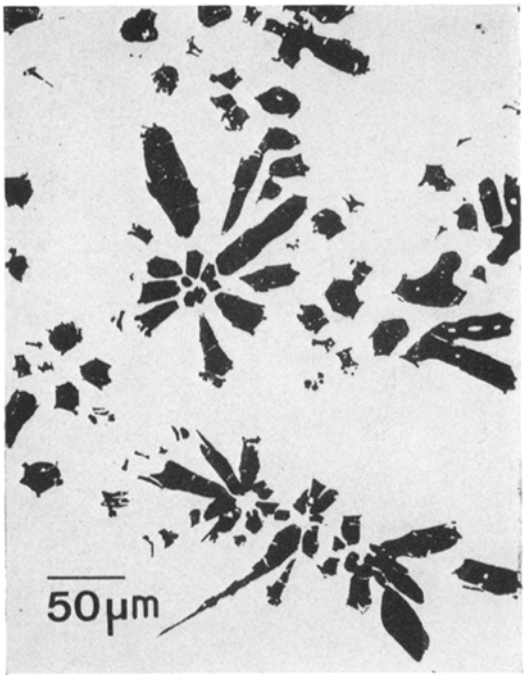

Figure 9 Primary faceted low-cristobalite crystallized from a hypereutectic melt (59%) held 70 min at 1450° C after cooling from 1600° C. (Because of low magnification the eutectic structure is not visible in the background.)

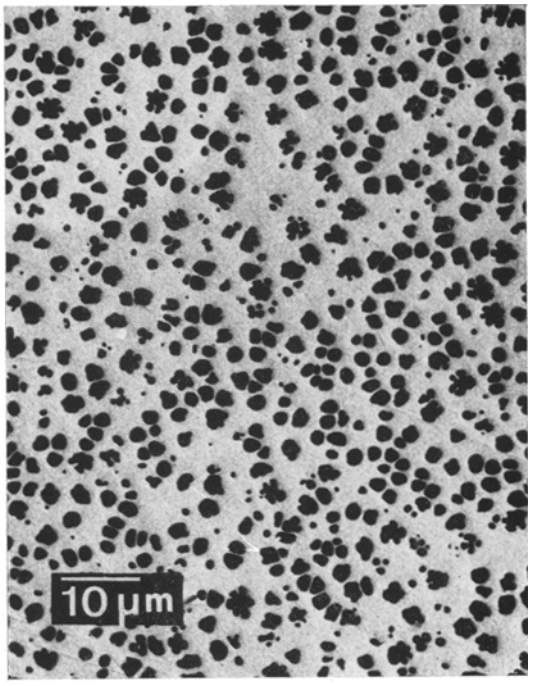

Figure 10 Hypereutectic melt (59%) after rapid cooling (condition 1). The eutectic structure between primary amorphous B-particles (dark) is not resolved by PEEM.

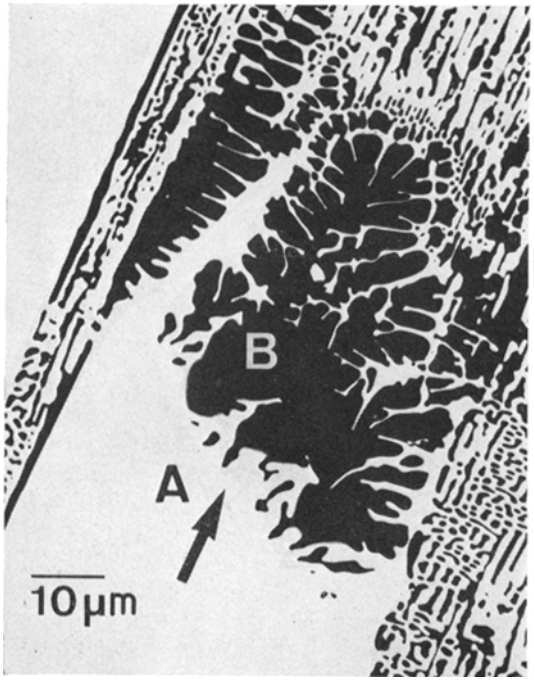

Figure 11 Eutectic melt (51%) after slow cooling (condition 4). During growth of large A-crystals (A, α-form, arrow indicates growth direction), an SiO_2-rich phase is accumulated forming curved dendrites (B). (In order to obtain a clear contrast, this picture is underexposed, thus A appears homogeneous.)

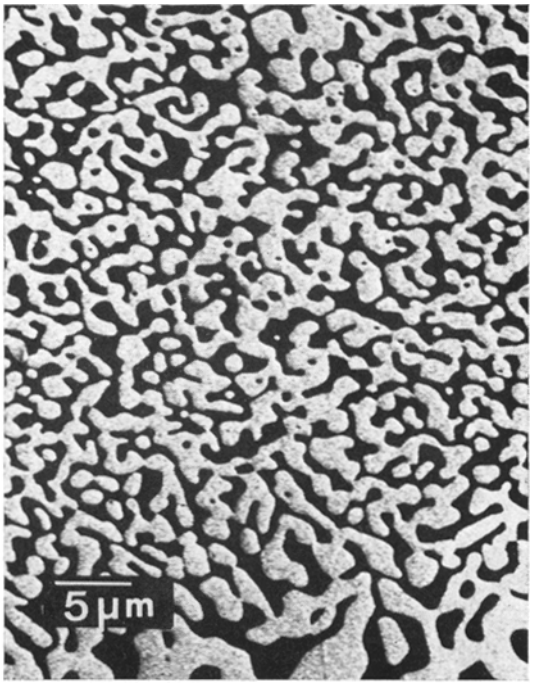

Figure 12 Eutectic morphology between large A-crystals as in Fig. 11 (cf. Fig. 2, C).

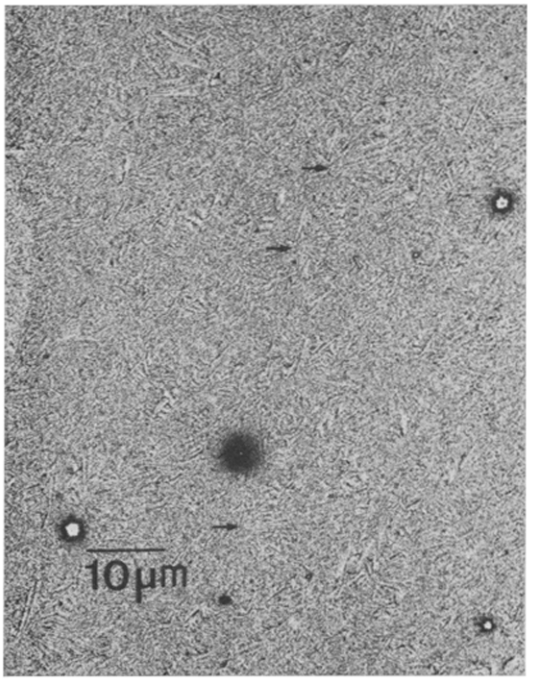

Figure 13 Eutectic structure after solidification in the "coupled region" (cooling condition 3). Partially spherulitic formation of phase A (β-form, small arrows), besides amorphous phase B (dark). (The large bright and dark spots are artefacts.)

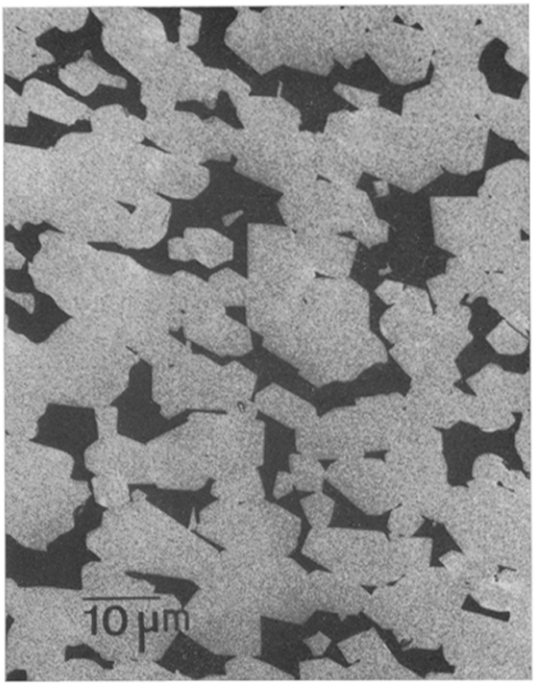

Figure 14 A glassy eutectic sample reheated at 1400 to 1420°C (condition 5). Between A-crystals (bright, α-form) there is an SiO_2-rich phase in the interspace (dark, low-cristobalite).

slowly (condition 4) structures as in Figs. 11 and 12 are developed. Phase A grows as the first eutectic constituent, while the surrounding undercooled liquid is simultaneously enriched in SiO_2, especially at the growth fronts of the idiomorphic A-crystals (Fig. 11). This process is comparable to that of zone refining and has been called "divorced eutectic" [17].

In the regions between the A-crystals of the same sample, another structure is developed (Fig. 12), where the A-phase is more irregularly shaped. This sample gives X-ray evidence of α-zinc silicate and low-cristobalite. The appearance of Fig. 12 is observed to be characteristic of the eutectic structure as well as primary A-crystals grown from a hypoeutectic melt (Fig. 2). A eutectic melt when cooled more quickly (conditions 2 and 3), enters the eutectic "coupled region" (E, Fig. 1) where crystallization of phase A (in the β-form) and formation of amorphous B, occurs simultaneously. This gives rise to the finely divided eutectic structure (Fig. 13) very similar to those of hypereutectic samples (Figs. 7 and 8) cooled under the same conditions (i.e. 2 and 3). The more rapidly eutectic and hypereutectic samples are cooled, the finer the resulting eutectic structure.

Crystallization of the β-form of phase A seems to be favoured to that of the stable α-form if the liquid-to-solid transition requires short-range diffusion, either during very rapid cooling of hypoeutectic melts or during the first steps of the common formation of phases A and B in the eutectic "coupled region". The reason is seen in the structural similarity [9] of liquid zinc silicate melt and β-zinc silicate. Both are assumed to contain Zn^{2+} with the less usual six-fold oxygen co-ordination. α-Zn_2SiO_4 contains Zn^{2+} only in the four-fold co-ordination and obviously needs more time to form. Only small globules ($\approx$ 0.5 µm) of phase B can be observed in rapidly cooled eutectic samples as a consequence of the metastable liquid miscibility gap extending into the eutectic region at low temperatures. The samples are then glassy with the beginnings of crystallization of β-zinc silicate (cf. Fig. 10).

A coarse, regular morphology (Fig. 14) arises from the devitrification of such glassy samples during reheating at 1400 to 1420°C (condition

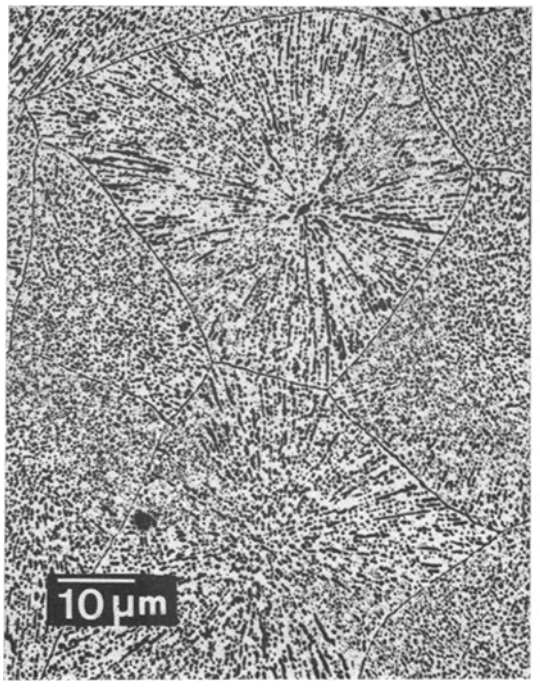

Figure 15 Glassy eutectic sample reheated at 1350°C (condition 6). Colonial grain structure formed by cellular growth.

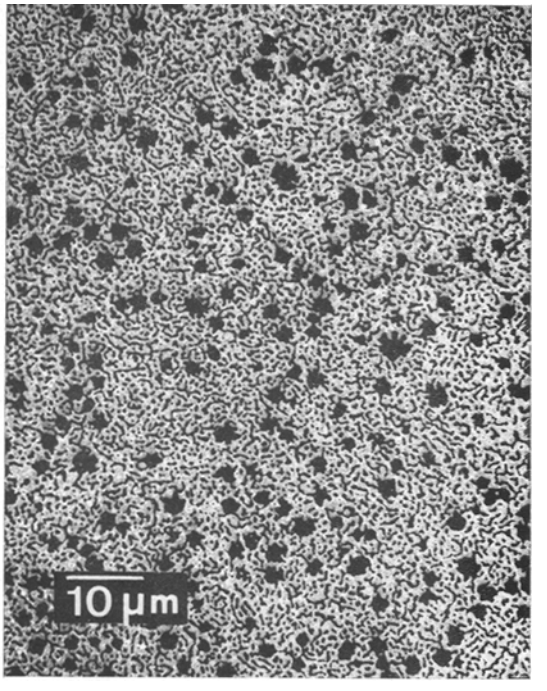

Figure 16 Glassy hypereutectic sample (54%) reheated at 1350°C (condition 6). Primary B-particles (dark) did not dissolve as in the eutectic sample (Fig. 15) but have grown further within a phase morphology which may also appear similar to Fig. 15.

5). It consists of interconnected idiomorphic A-crystals and SiO_2-rich phase in the interspace. α-zinc silicate and low-cristobalite are the crystalline phases present. It should be noticed that coarse eutectic structures as seen in Figs. 11, 12 and 14 arise just below the eutectic temperature and outside the metastable region of liquid immiscibility (Fig. 1). If a glassy eutectic sample is reheated at a lower temperature (1350°C, condition 6), a grain structure develops, the boundaries of which are indicated by deposition of a SiO_2-rich phase. Grains, as shown in Fig. 15, seem to arise from a colony formation which is known to come from cellular solid–liquid interface topography during growth [1]. Cellular growth [1, 19] is caused by constitutional undercooling of the liquid ahead of the advancing growth front of dendritically growing phase A separating SiO_2. The growth mechanism is comparable to that working in the eutectic liquid around primary A-crystals after rapid cooling of hypoeutectic samples from 1440°C (Fig. 4).

According to the phase diagram (Fig. 1), the structure of Fig. 15 was formed just at the boundary of the metastable field of liquid immiscibility and hence most of the B-particles formed earlier (see Fig. 10) have been dissolved The same procedure applied to a hypereutectic composition (54%) does not dissolve B-particles but even causes them to grow further (Fig. 16). Corresponding to these morphological observations, there is clear X-ray evidence of low-cristobalite in the latter sample, but only poor indication in that of the eutectic (Fig. 15).

5. Conclusions

(1) In the system Zn_2SiO_4–SiO_2, α-zinc silicate may take up approximately 3% excess SiO_2 if grown from a hypoeutectic melt above the eutectic temperature and crystallizes with an idiomorphic pseudo-hexagonal habit. If grown from a rapidly cooled melt (condition 1) the habit is strongly deformed. Moreover, the crystalline α-form may be replaced by the metastable β-form and the cooling rate necessary to obtain the latter from a hypoeutectic melt decreases as the eutectic composition is approached.

The limited Zn_2SiO_4–SiO_2 solid solution is called phase A comprising both crystalline polymorphs. The composition of phase A is

assumed to change according to line a, Fig. 1, if grown from rapidly cooled melts. The additional SiO_2 content does not change the *d*-spacings of the X-ray diagram of both zinc silicate polymorphs. Cooling to room temperature yields SiO_2 segregation on a fine scale as seen by PEEM.

(2) Phase intergrowth morphologies of hypereutectic compositions after solidification from the melt are determined by the metastable region of liquid immiscibility (Fig. 1). Primary amorphous phase B (SiO_2-rich) appears as small particles which tend to coalesce to form curved dendrites. Between these B-particles there is a very fine eutectic structure consisting of phase A (β-form) and amorphous phase B (Figs. 7 and 8). The SiO_2-rich phase crystallizes as low-cristobalite during slow cooling.

(3) Eutectic phase intergrowth morphology of slow solidification is determined by the growth of large A-crystals (α-form) from the undercooled liquid which is simultaneously enriched in SiO_2. The kinetics resemble the process of zone refining and lead to a so-called "divorced eutectic" [17].

In regions between larger A-crystals, a different eutectic morphology develops (Fig. 12), which is also typical in slowly cooled hypoeutectic samples (Fig. 2). At medium cooling rates (conditions 2 and 3), solidification takes place in the eutectic "coupled region" (E, Fig. 1) producing a very finely divided structure consisting of phases A (β-form) and B (amorphous). After rapid cooling (condition 1) the eutectic melts formed are mostly in the glassy state. Only the globules of phase B are visible by PEEM while the background is not resolved.

Re-heating the glassy samples at 1400 to 1420° C yields a coarse structure (Fig. 14) while heating at 1350° C gives rise to a finer colonial grain structure (Fig. 15). In hypereutectic samples, the temperature has the same effect on the resulting morphologies.

Acknowledgements

We thank Mr R. Gubser (Institut für Kristallographie und Petrographie, ETH, Zürich) for providing the electron microprobe measurements. Thanks are also due to Miss E. Grauer-Carstensen for technical assistance in photoemission electron microscopy. Financial support by the Swiss Commission for the Encouragement of Scientific Research (proj. No. 791) is gratefully acknowledged.

References

1. G. A. CHADWICK, *Prog. Mat. Sci.* **12** (1963) 99.
2. L. M. HOGAN, R. W. KRAFT and F. D. LEMKEY, *Adv. Mat. Res.* **5** (1971) 83.
3. F. L. KENNARD, R. C. BRADT and V. S. STUBICAN, *J. Amer. Ceram. Soc.* **56** (1973) 566.
4. L. WEGMANN, *J. Microscopy* **96** (1972) 1.
5. K. H. GAUKLER and R. SCHWARZER, *Messtechn.* **81** (10) (1973) 307.
6. CH. ZAMINER, *Optik* **31** (1970) 116.
7. L. WEBER, *Schweiz. Min. Petr. Mitt.* **52** (1972) 349.
8. E. N. BUNTING, *J. Nat. Bur. Stand.* **4** (1930) 131.
9. J. WILLIAMSON and F. P. GLASSER, *Phys. Chem. Glasses* **5** (1964) 52.
10. H. P. ROOKSBY and A. H. MCKEAG, *Trans. Faraday Soc.* **37** (1941) 308.
11. H. F. W. TAYLOR, *Amer. Minerol.* **47** (1962) 932.
12. A. SCHLEEDE and A. GRUHL, *Z. Elektroch.* **29** (1923) 411.
13. G. R. FONDA, *J. Phys. Chem.* **44** (1940) 851.
14. K. A. JACKSON, "Liquid metals and solidification" (ASM, Cleveland, Ohio, 1958).
15. J. D. HUNT and K. A. JACKSON, *Trans. Met. Soc. AIME* **236** (1966) 843.
16. O. W. FLOERKE, *Fortschr. Min.* **44** (1967) 181.
17. P. GORDON, "Principles of phase diagrams in materials systems" (McGraw-Hill, New York, 1968).
18. B. E. SUNDQUIST, R. BRUSCATO and L. F. MONDOLFO, *J. Inst. Metals* **91** (1962-63) 204.
19. H. M. WEART and D. J. MACK, *Trans. Met. Soc. AIME* **212** (1958) 664.

Received 16 October and accepted 28 November 1974.